DD

Research Center for the Early Universe

The University of Tokyo

RESCEU No.35/96

Astro-E hard X-ray detector

T.Kamae*, H.Ezawa, Y.Fukazawa*, M.Hirayama*, E.Idesawa, N.Iyomoto, H.Kaneda, G.Kawaguti, M.Kokubun, H.Kubo, A.Kubota, K.Matsushita, K.Matsuzaki, K. Makishima*, T.Mizuno, K.Nakazawa, S.Osone, H. Obayashi, Y.Saito, T.Tamura, M.Tanaka, M.Tashiro*,

Department of Physics, University of Tokyo
(*) also *Research Center for the Early Universe, Univ. of Tokyo*
Hongo 7-3-1, Bunkyo-ku, Tokyo 113, Japan

J.Kataoka, T. Murakami, N.Ota, H.Ozawa, M.Sugizaki, K.Takizawa, T.Takahashi, K.Yamaoka

Institute of Space and Astronautical Science
Yoshinodai, Sagamihara, Kanagawa 229, Japan

A. Yoshida

Institute of Physical and Chemical Research (RIKEN)
2-1 Hirosawa, Wako, Saitama 351-01, Japan

H. Ikeda and K. Tsukada

National Lab. for High Energy Physics (KEK)
Ohomachi, Tsukuba-city, Ibaraki 305, Japan

M. Nomachi

Research Center for Nuclear Physics, Osaka University
Mihogaoka, Ibaraki-shi, Osaka 567, Japan

Presented in a SPIE 1996 International Symposium
on
"Gamma-Ray and Cosmic Ray Detectors, Techniques and Mission"

To appear in SPIE proceeding

Research Center for the Early Universe (*RESCEU*)
Faculty of Science, The University of Tokyo, Bunkyo-ku, Tokyo 113, Japan
FAX: +81–3–5684–5291

Astro-E hard X-ray detector

T.Kamae*, H.Ezawa, Y.Fukazawa*, M.Hirayama*, E.Idesawa, N.Iyomoto, H.Kaneda, G.Kawaguti, M.Kokubun, H.Kubo, A.Kubota, K.Matsushita, K.Matsuzaki, K. Makishima*, T.Mizuno, K.Nakazawa, S.Osone, H. Obayashi, Y.Saito, T.Tamura, M.Tanaka, M.Tashiro*,

Department of Physics, University of Tokyo
(*) also *Research Center for the Early Universe, Univ. of Tokyo*
Hongo 7-3-1, Bunkyo-ku, Tokyo 113, Japan

J.Kataoka, T. Murakami, N.Ota, H.Ozawa, M.Sugizaki, K.Takizawa, T.Takahashi, K.Yamaoka

Institute of Space and Astronautical Science
Yoshinodai, Sagamihara, Kanagawa 229, Japan

A. Yoshida

Institute of Physical and Chemical Research (RIKEN)
2-1 Hirosawa, Wako, Saitama 351-01, Japan

H. Ikeda and K. Tsukada

National Lab. for High Energy Physics (KEK)
Ohomachi, Tsukuba-city, Ibaraki 305, Japan

M. Nomachi

Research Center for Nuclear Physics, Osaka University
Mihogaoka, Ibaraki-shi, Osaka 567, Japan

ABSTRACT

Astro-E is the X-ray satellite to be launched in year 2000 by Inst. of Space & Astronautical Science. This report deals with the design and expected performance of the Hard X-ray Detector (HXD), one of the 3 experiments aboard Astro-E. The HXD is a combination of GSO/BGO well-type phoswich counters and silicon PIN diodes: the two combined will cover a wide energy band of 10−700 keV. The detector is characterized by its low background of $\sim 10^{-5}$/s/cm^2/keV and its sensitivity higher than any past missions between a few 10 keV and several 100 keV. Combined with the other 2 experiments, a micro-calorimeter array (XRS) and 4 CCD arrays (XIS), both with X-ray mirrors, the mission will cover the soft and hard X-ray range at a highest sensitivity.

Keywords: X-ray astronomy, hard X-ray detector, phoswich counter, silicon PIN diode, Astro-E

1 ASTRO-E PROJECT

The fifth Japanese X-ray astronomy satellite, ASTRO-E, following *Hakucho*, *Tenma*, *Ginga*, and *ASCA*, is scheduled for launch in year 2000 by the new launcher M-V-4 of Institute of Space and Astronautical Science from ISAS Kagoshima Space Center.[1] This satellite will carry three experiments: the Hard X-ray Detector (HXD) covering the energy band from 10 keV to 700 keV; a micro-calorimeter array with an X-ray mirror (X-ray Spectrometer – XRS); 4 CCDs with 4 X-ray mirrors (X-ray Imaging Spectrometer – XIS). The latter two experiments cover the soft X-ray band with the highest energy resolution[2] (micro-calorimeter: $\Delta E \sim 12$eV), or with good energy resolution[3] (CCDs: $\Delta E \sim 150$eV at 5.9keV), both with imaging capability. All 3 experiments combined, Astro-E will become a spectrometer facility covering the energy band from 0.4 keV to 700 keV with good to moderate spatial resolution (XRS/XRT and XIS/XRT: $\sim$ 1 arcmin., HXD: $\sim$ 20 arcmin.).

The total weight and power available for the 3 experiments will be about 800kg and 200W, respectively. The M–V rocket will put the satellite into a near-circular orbit of radius 550km with an inclination of 31 deg. The 3 scientific instruments, the X-Ray Spectrometer (XRS) with an XRT (focal length $\sim$3.5m), the 4 X-ray Imaging Spectrometers (XIS) with an XRT each (focal length $\sim$4.5m), and the HXD, have adopted several new and inovative technologies. The micro-calorimeter array made of 36 HgTe elements will be the first such instrument to fly in a satellite and will have the ultimate energy resolution ($\sim$12eV) in the soft X-ray band.[2] The XRTs will be made of replica foils and will allow 1 arcmin. spatial resolution despite their light weight.[4] The X-ray CCDs will have deeper depletion region ($\sim$ 80 μm) and their energy resolution (fwhm) will reach the theoretical limit for the CCD: below 55eV at Oxygen K-line and 145 eV at 5.9 keV.[3] The large ($\sim$ 20mm$\times$20mm) 2mm-thick silicon PIN diodes used in the HXD will be the first of this kind and will give us an energy resolution about 3keV (fwhm) in the hard X-ray band ($\sim$ 10 to 70 keV). The well-type phoswich counter itself is a new concept and will use a newly developed fast and high light-yield inorganic scintillators GSO(Ce) in its detection part.[5] [6] [7] These instruments will be prepared by ISAS, Univ. of Tokyo, Osaka Univ., Kyoto Univ., Nagoya Univ., Tokyo Metropolitan Univ., RIKEN, NASA/GSFC, Univ. of Wisconsin, and MIT.

The time schedule of the project is as follows: the R/D works have nearly been completed in Japanese FY 1995, the Engineering Model (EM) of crucial items with its associated electronic circuitry have been produced and tested in the spring of 1996. Based on these tests and R/D works, the design will be frozen in the fall of 1996 and production of the Flight Model (FM) will begin early 1997. The FM will then be completed in mid-1998 followed by the final assembly and tests. The launch date is set at present late in Japanese FY 1999 or in the winter of calender year 2000.

2 ASTRO-E HARD X-RAY DETECTOR

The Astro-E HXD[8] [9] has been jointly developed by scientists at Department of Physics, University of Tokyo, Institute of Space and Astronautical Sciences (ISAS), Institute of Physical and Chemical Research (RIKEN), National Laboratory for High Energy Physics (KEK), and others. It is basically an upgraded version of the well-type phoswich counters successfully flown on balloons.[10] [11] [12] [13] [14] [15] Silicon PIN diodes are the important addition introduced to lower the energy coverage as well as to improve the energy resolution in the lower energy band. The design and characteristics of the HXD as of June 1996 are described here together with its expected performances.

The HXD detector assembly is schematically shown in Fig. 1. The total weight of this assembly will be about 200 kg including the electronic part not shown in the figure. The HXD consists of 16 (=4$\times$4) modular units and has an overall photon collecting area of about 330 cm^2. Each unit is built around a phoswich counter made of a fast inorganic scintillator, GSO (Gd_2SiO_5:Ce 0.5% mol)[5] [6] [7] and the BGO active shield as shown in Fig. 2. Cosmic hard X-rays are detected as clean-hits if their full energy is deposited in the fast scintillator GSO. The active collimation part of the BGO shield forms four deep-wells (320mm deep, $\sim$25mm $\times$ 25mm in area), limiting the field of view to $\sim 4.3° \times 4.3°$. The GSO crystals (four per unit, each measuring in area 24 mm$\times$24 mm and in thickness 5 mm) are glued at the bottom surface of the wells. The

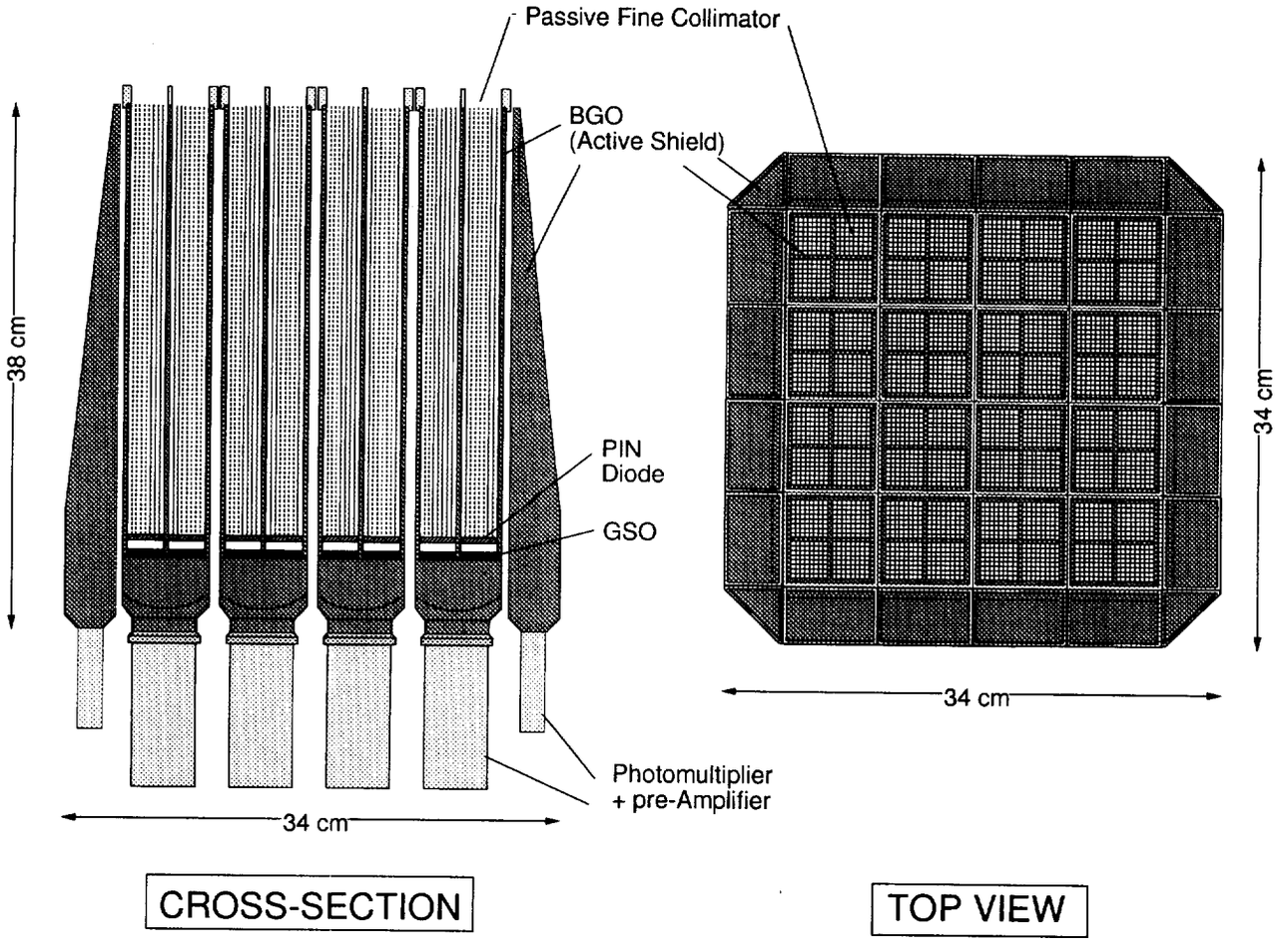

Figure 1: The HXD detector assembly: Cross-section (left) and the top view (right). The housing and most of the electronic part are not shown here.

entire assembly is viewed by a 2-inch phototube from the exterior surface of the shielding part.

The silicon PIN diodes, each with an active area of 20 mm×20 mm×2 mm, are assembled in a unit of two layers and placed in the deep BGO well just above the detection part (Fig. 2). Two PIN diodes are placed per well, making a total of eight per unit. The HXD contains 128 Si diodes in all, achieving a photon collecting area of about 230 cm^2.

Each group of 4 detector units will be equipped with an independent high voltage supply for the phototube, and a common DC power supply for 8 PIN diodes. Fig. 3 shows the effective areas of the phoswich scintillators and the silicon PIN diodes, in the respective energy ranges of $40 - 700$ keV and $10 - 70$ keV.

The 4×4 matrix of phoswich counters are surrounded by 20 units of thick BGO anti-counters for additional shielding. Furthuremore, a fine collimator made of phosphor bronze sheet (50μm thick) is placed inside the BGO wells to match the HXD field of view to that of the soft X-ray telescopes (17×17 $arcmin^2$). This collimeter is expected to reduce the the cosmic diffuse X-ray background that may otherwise become a dominant background source for the PIN diodes. In the soft γ-ray band, background is reduced by mutual anti-coincidence among neighboring units. We expect the detector background to be below 10^{-5} $c/s/cm^2/keV$ for the Si PIN diodes and $\sim 10^{-5}$ $c/s/cm^2/keV$ for the scintillators.

The estimated sensitivity will be set by the background due to the radioactivity induced within the counters while in the orbit. It will be substantially better if the detector is flown in a lower orbit (eg. that of CGRO), where activation is much less. than the ultimate limit the well-type phoswich counter can attain. Lowering the background and knowing its origins are crucial in the following respect: We plan to avoid the

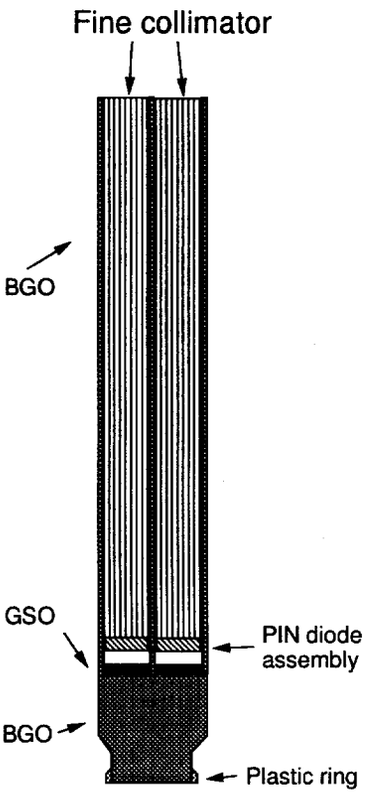

Figure 2: Cross-section of one HXD detector unit.

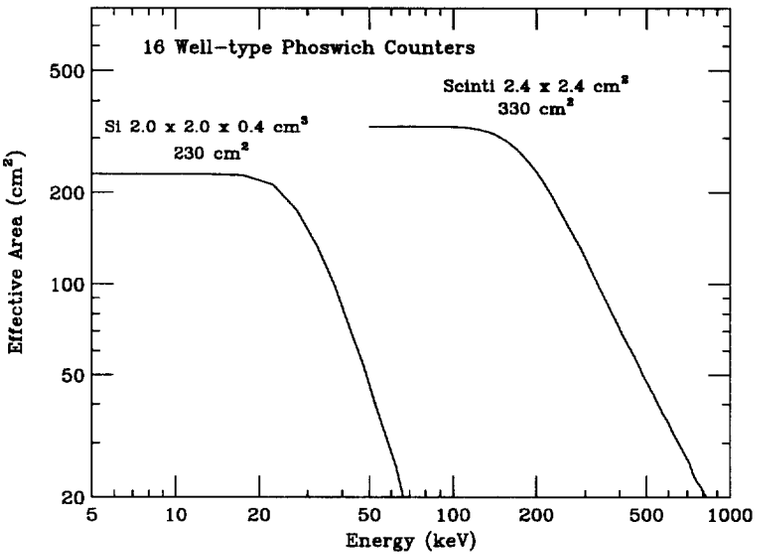

Figure 3: Effective area of the HXD: The geometrical area of the GSO scintillators (5 mm thick) is 368 cm^2 and that of the silicon PIN diodes (4 mm thick) is 256 cm^2. With the fine collimator, the two effective areas are reduced by about 10 % to become 330 cm^2 and 230 cm^2, respectively.

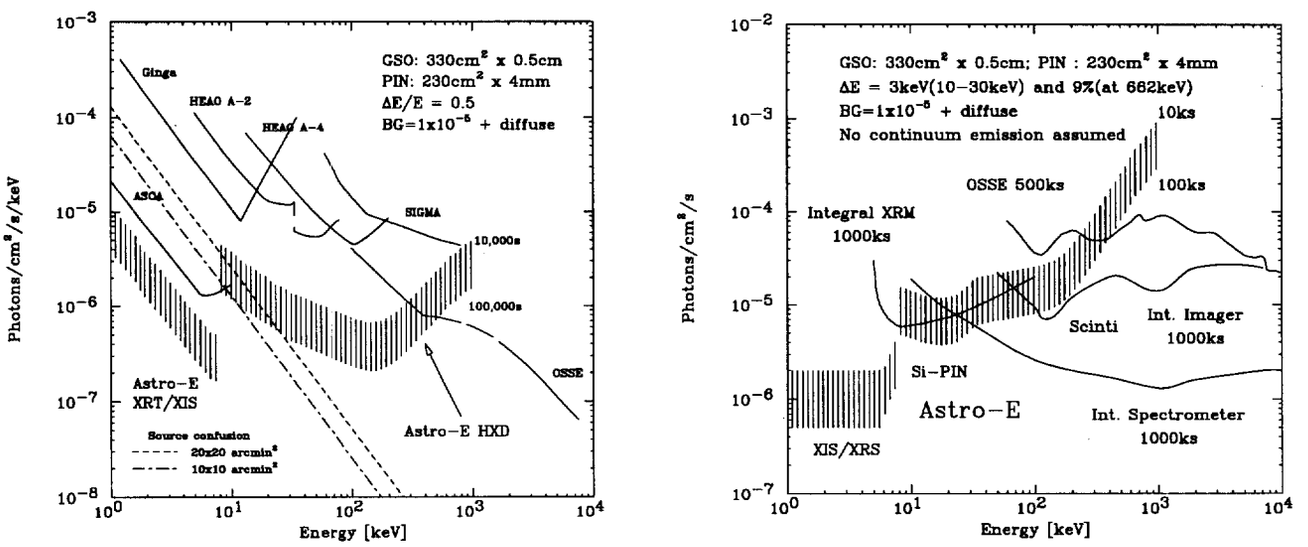

Figure 4: Sensitivities (3σ) to the continuum (left) and line (right) emissions of Astro-E HXD and selected missions.

ON-OFF subtraction by estimating the background accurately ($\sim$ a few %) from monitor counts as was done in the Ginga LAC observations.[16]

In Fig. 4, the expected 3σ sensitivities to the continuum and to the line emission of Astro-E HXD are compared with those of the past and planned satellite missions. The sensitivity of Astro-E HXD for point sources will be substantially higher than any other past missions in the energy band between 10 keV to several 100 keV. We therefore expect to detect and study many new cosmic hard X-ray point sources. The Astro-E HXD, on the other hand, will have only a modest sensitivity to diffuse gamma-ray emissions such as the 511 keV line distributed over the Galactic ridge.

2.1 Well-Type Phoswich Array

The phoswich counter consists of two kinds of scintillators whose scintillation decay times are distinclty different. The faster scintillator is placed in the front as the detection part and the slower one in the back as the shielding part. The phototube signals generated purely by the faster scintillator are selected by using an appropiate pulse-shape discriminator (PSD). Signals with an appreciable contribution from the slower scintillator, eg. those of hard X-rays scattered by the shielding part and those of charged particles penetrated through the shielding part, are efficiently rejected (see Sec.4.3). This phoswich technique has been used for many years in cosmic γ-ray detection. The uniqueness of the "well-type" phoswich counters is that the well-shaped shielding part acts also as an active collimator and that each counter filters out, quickly and effectively, unwanted hard X-rays down if even only a small energy ($50 - 100$keV) is deposited in the collimator and shielding part.[10] [12] The detection part (the fast scintillator) being buried deep in the active anti-coincidence well also reduces efficiently background due to nuclear activity. The details on the development of the well-type phoswich counter are given elsewhere.[10] [11] [12] [13]

Choice of the two scintillation materials becomes important in reducing the background and improving energy resolution. For its large effective atomic number and long scintillation decay time, BGO emergied as the choice for the shielding part. Through a test on a prototype well, we noted that BGO commercially available at that time was contaminated by a radioactive isotope ^{207}Bi.[17] [18] [12] A prior report existed finding that the amount of contamination largely depends on where the Bi ore comes from.[18] The BGO scintillators now commercially available have substantially reduced ^{207}Bi contamination..[19]

Radioactive contamination (natural and induced) in the detection part contributes to the background more directly and should be absolutely minimized. Radioactive contamination has been measured for two high-light-yield scintillation materials with fast decay times, GSO(Ce)[5] [6] and YAP(Ce)[20] [21] (see Table 1), and their activation characteristics have been studied by irradiating them with protons of kinetic energies typical to the satellite orbit ($\sim$100 MeV).[10] [12] [22] [23] The study has shown that the number of long-life line γ-rays in the energy range of HXD is comparable for 2 cm thick YAP and 5 mm GSO for a fixed dose of proton. Note that the radiation length is quite different for the two crystals (see Table 1). We found recently that scintillation light yield decreases as temperature drops below 0°C for YAP but increases for GSO as shown in Fig. 5.[7] We also found that a slowly decaying scintillation component becomes dominant below 0°C for YAP.[7] We plan to set the operating temperature at around $-15 \sim -20$°C so that the leakage current of the PIN diodes be reduced: hence GSO(Ce) became our final choice.

We have already received about 40 GSO scintillators from Hitachi Chemical: their light yield are around 30% of a typical NaI(Tl) and give about $\Delta E(fwhm) \simeq 6.8 - 7.5\%$ at 662 keV when directly coupled to the PMT. When viewed through the BGO well, the resolution deteriorates typically to $\simeq 9.5\%$ at 662 keV at room temperature. Since the light yield is expected to increase by about $\sim 15\%$ in the operating temperature (-20°C) as seen in Fig. 5, we expect the resolution to be around $\Delta E(fwhm) \simeq 8.8\%$ or $\simeq 7\%/\sqrt{E[\mathrm{MeV}]}$.

2.1.1 Fine collimator

The two other experiments in the Astro E mission focuss on fine spectroscopy with imaging capability and have a narrow field of view (FOV) of around 17×17 arcmin^2. The FOV of HXD is determined by

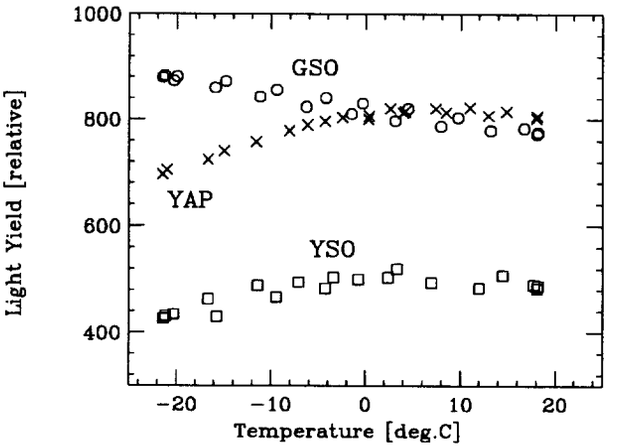

Figure 5: Temperature dependence of light yield for GSO, YSO and YAP when measured with a shaping amplifier with 500 ns time constant.

Table 1: Characteristics of NaI, BGO, GSO and YAP

Chemical composition	NaI(Tℓ) NaI (Tℓ)	BGO $Bi_4Ge_3O_{12}$	GSO(Ce) Gd_2SiO_5 (Ce)	YAP(Ce) $YAlO_3$ (Ce)
Eff. atomic number	50	74	59	35
Density (g/cm^3)	3.7	7.1	6.7	5.5
Rad. length (cm)	2.6	1.2	1.4	2.6
Index of refraction	1.85	2.15	1.9	1.94
At around 20°C				
Decay time (ns)	~230	~300	~60	~30
Light yield (relative)	100	~12	~28	~35
Peak emission (nm)	410	480	430	347
At around −20°C: data on GSO and YAP are preliminary.				
Decay time (ns)	~500	~600	~80	~30 and > 500
Light yield (relative)	~75	~15	~30	~20
Peak emission (nm)				

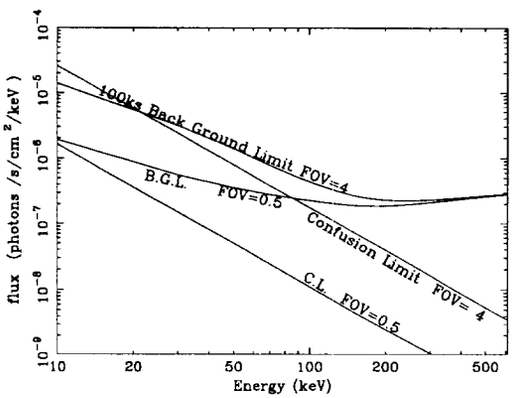

Figure 6: Limit to the sensitivity set by the diffuse background (B.G.L.) and source confusion (C. L.), with the 8 × 8 fine collimator (FOV=0.5) and without (FOV=4).

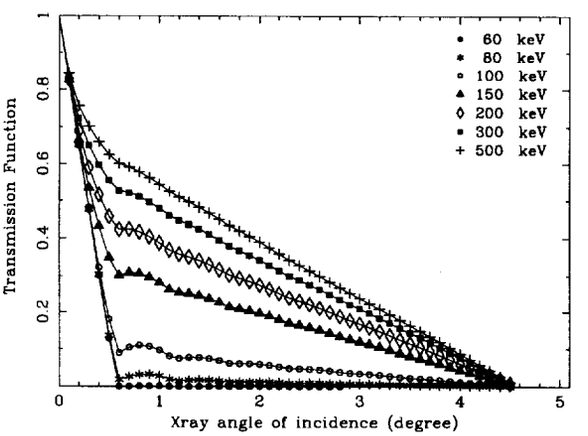

Figure 7: Transmission function of the fine collimator.

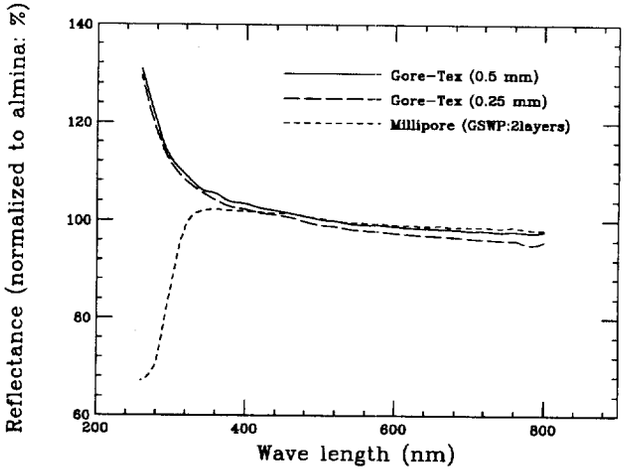

Figure 8: Reflectivity of reflective sheets as a function of wavelength.

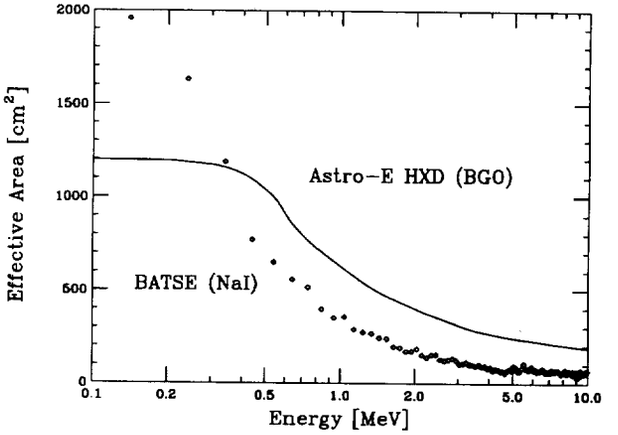

Figure 9: Effective area of one of the 4 anit-counter planes used as the γ-ray burst detector (BGO 2.6 cm) compared with that of BATSE one unit.

the depth of the BGO well and the cell size of the fine colimator, both of which are in principle adjustable. In practice, however, the mechanical stability and availability of the BGO crystal set a limit at around the present value of 32 cm. The transverse dimension of the detection part is required to be substantially larger than the depth, setting the FOV at around 4.3 deg. At the low background rate of the well-type phoswich counter, the sensitivity will then be limited by the source confusion and diffuse background for the 4.3 deg FOV up to about 100 keV (see Fig. 6).[24] The passive fine collimator has been designed to reduce the source confusion and diffuse background.[24]

The collimator is made of phosphorus blonze sheets spot-welded to form 30 cm long 8×8 cells. The thickness of the phosphorus blonze sheets is 50μm which gives a narrow FOV below 100 keV but secures an order of magnitude wider FOV for the 511 keV line (see Fig. 7).

The challenge we now face is accuracy of the cell-to-cell alignment as well as the mutual alignment of the 4 collimators in a detector unit. Possible nuclear activation of phosphorus blonze in orbit also concerns us and will be studied by irradiating the material with 100 MeV protons.

2.1.2 UV-tansparent epoxy and reflector

The shielding part (the well and the bottom in Fig. 2) is made of seven BGO plates and a BGO block: they are glued together by epoxy resin transparent in $\lambda \sim 350 - 600$ nm, EpoTek 301−2 by Epoxy Technology Inc.[25] [26] The detection part, GSO, is glued by silicon compound KE103 by Shin'Etsu Chemical[27] that can absorb the difference in the expansion coefficients of BGO and GSO ($\sim 10^{-5}$ in one axis). It is also transparent in the wavelength range.[25]

The scintillator assembly is then wrapped by a light reflector sheet that has a high reflectance in the wave band and chemically stable. Our test has shown that the white GorTex sheet[28] has the best reflectance as shown in Fig. 8.

2.2 Anti-Counters

The anti-counters serve primarily to guard the 16 well-type phoswich counters from nuclear particle bombardment and to reduce the background in the phoswich counters (see Fig. 1). They are made of BGO and have wedge shapes as shown in the figure. Combination of these 20 anti-counters and the shielding parts shields all GSO scintillators with at least $\sim$5 cm of BGO all around. This reduced the cosmic proton flux

on the GSOs by an order of maginitude.[23] The anti-counters also serve to reduce Compton scattered events as well as nuclear activation background events.

The total area covered by these thick BGO anti counters (2.6 cm in average) is quite impressive: each face has a geometrical area of ~1200 cm^2. and an effective area at 1 MeV of ~600 cm^2 as shown in Fig. 9. We plan to use all 4 faces to monitor γ-ray bursts and transient phenomena. By comparing the counts in the 4 faces, we will be able to determine the direction to $\sim 5°$.

Because of the scintillator shapes, we do not expect a good energy resolution in this monitor. The energy range coverage, on the other hand, will be quite wide as shown in Fig. 9. The scintillator used (BGO) is relatively fast and allows us to record transient phenomena in fine time bins (1/64 ms) as will be discussed in Sec.4.1. We believe this will be quite important when locating γ-ray bursts by the arrival times registered by 3 or more satellites, one being Astro-E.

2.3 Silicon PIN Diode

In the well-type phoswich counter, two layers of 2 mm thick PIN diodes sit in front of the GSO scintillators. Softer X-rays will be photo-asborbed in the two layers of PIN diodes, while harder photons pass through the two diode layers and reach the GSO crystal (see Fig. 3).

The PIN diodes are introduced to fill the possible gap in the energy coverage between the phoswich counters ($\geq$ 50 keV) and the CCDs ($\leq$ 10 keV). The BGO wells provide the PIN detectors with a very low background environment and the diodes, in return, act as anti-coincidence shields for the scintillators against low-energy charged particles. The background level is expected to be substantially lower than 10^{-5}/sec/cm^2/keV for the PIN diodes.

There are several technically critical issues in developing thick PIN diodes. One needs ultra high purity (~ ultra high resistivity) silicon wafers that give little volume leakage current.[8] [29] [30] Even with such wafers, extreme care must be taken in the diode fabrication process not to increase edge leakage current nor to lower the breakdown voltage.[31] [32] Sample diodes with thickness of 1-1.5 mm have been produced by Hamamatsu, Micron, and Seiko Instruments Inc.[31] [32] We plan to develope 2 mm thick diodes and stack two of them to obtain 4 mm effective thickness. To reduce the leakage current to a reasonable level (< a few nA), we plan to operate HXD at around $-20°$C.

2.4 Low Noise Charge Amplifier

Improving the energy resolution is the most demanding issue in developing our silicon PIN diode. The energy resolution can be improved by optimizing the design of the preamplifier and the shaper amplifier. In reality, however, the total input capacitance (C_{in}) which is the sum of the junction capacitances of two PIN diodes (~ 2×20 pF) and the capacitance of the cables connecting the diodes to the preamplifiers (~ 30 pF) will determine the resolution.[8] [29] [30] We currently set our goal at an energy resolution of $\Delta E(fwhm) \simeq 3$ keV at $-20°$C and are developing a low-power low-noise amplifier system optimized to this large input capacitance. The current design gives the equivalent noise figure shown in Fig. 10.

3 HOUSING OF THE DETECTOR ARRAY

The mechanical vibration and shock is expected to be much higher for the M−V rocket of ISAS than for rackets powered by liquid fuel and the housing for the detector array requires great care. The dissipation of the heat generated by the AE parts placed in the housing (~ 15 W) poses additional constraint to the design. Since the BGO crystal is quite brittle, some support mechanism must be installed to damp external vibrations and to minimize the internal stress of BGO. The thermal expansion coefficient of BGO is an order

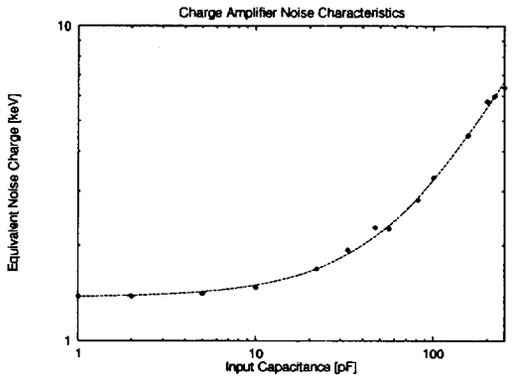

Figure 10: Equivalent noise count (ENC) of the preamplifier for PIN diodes.

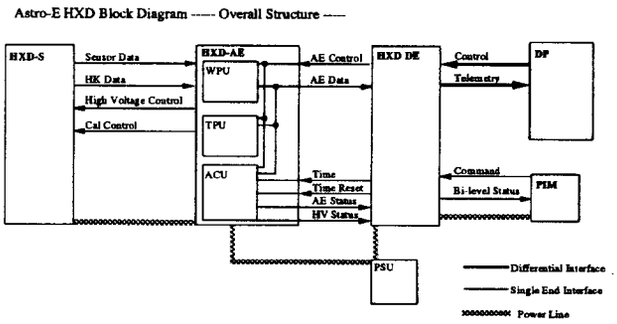

Figure 11: Block diagram of the HXD electronics

of magnitude smaller than any metal and consequently some critical parts will be made of carbon fiber or glass fiber reinforced plastic composite.

The detector array will probably be serviced including replacement of some detector units. This requires each unit to be mechanically independent. On top of all the above, the total amount of passive material must be minimized because of background generated by bombardment of cosmic protons and neutrons.

4 ELECTRONICS AND DATA ACQUISITION

The electronic system for the Astro-E HXD consists of the analog electronics part (AE) and the digital electronics part (DE)[9] as shown in Fig. 11. The AE consists primarily of pulse shape discriminators (PSD) and circuits associated with ADCs. The DE formats and processed the digitized data. The final data are then transmitted to the ground stations under control of DE. Data from various environmental monitors will also become critical in the HXD analysis, because the scintillation light yield is known to be temperature dependent and reliable background subtraction requires accurate monitoring of possible background origins.

4.1 Analog Electronics

The AE consists of one control board (ACU) and eight signal-processing boards (see Fig. 11). The latter are broken into the following two types: WPU for the well-type phoswich counters and PIN diodes, and TPU for the anti counters. The ACU handles power supply to AE and monitors the house keeping data about power supplies, timing, temperatures, and others.

The analog signal is taken from the last or the second last dynode of the PMT in the well-type phoswich counter. It is first fed to a charge sensitive preamplifier placed in the detector housing and then to a pulse shape discriminator (PSD) in the WPU board. The anode signal of the PMT is used for a fast pre-trigger that generates the peak-hold gate for the PSD. The PSD selects signals whose time profiles are consistent with that of the detection part (GSO), and rejects those contaminated with slow-decaying BGO scintillation light. While in orbit, the counting rate in the shielding part will be 4-5 orders of magnitude higher than that of clean hits in the detection part. The PSD selects the clean hits by comparing the output pulse heights from the two shaping amplifiers with different integration times. The PSD has been developed as a semi-customed LSI to reduce the circuit size and power consumption.[33] [34] [35]

PIN diodes can also trigger the data aquisition system if a diode level discriminator detects a signal while no slow scintillation light is detected by the PSD for the phoswich unit housing the diode.

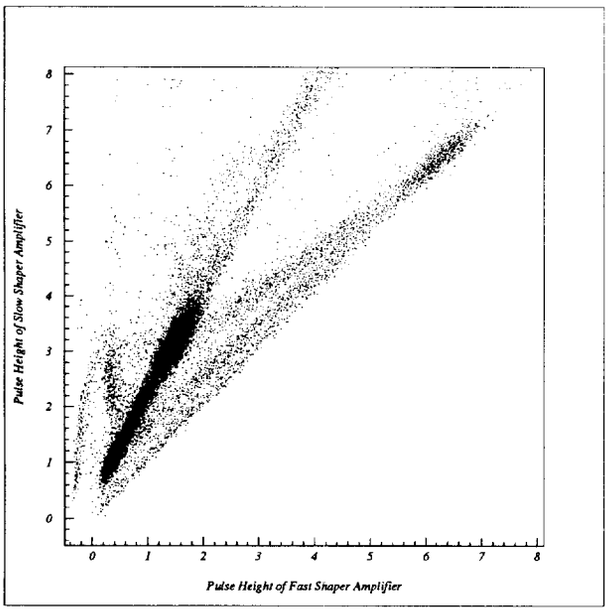

Figure 12: Correlation between the fast and slow shaper outputs (τ = 100 ns and 500 ns) obtained by the EM unit at $-20°$ deg. and the PSD LSI irradiated by 662 keV gamma-rays. See text.

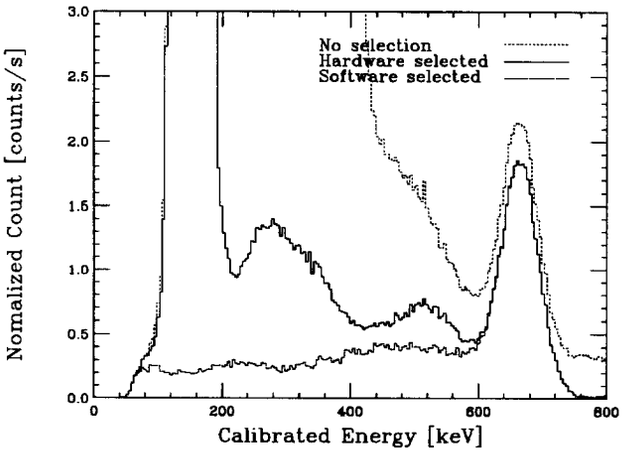

Figure 13: Pulse height distribution of the slow shaper output selected by the PSD gate and offline filtering from Fig. 12. Since the data was taken with only one unit and in a temperature control box, gamma-rays escaped through the 3 mm BGO wall after hitting GSO and stray gamma-rays entered through the 3 mm BGO wall to hit GSO.

When a trigger is issued either by a PSD or a PIN diode, all analog outputs from the corresponding phoswich unit (those of the slow shaper, the fast shaper, and the four diode shapers) are digitized. The upper discriminator outputs (see below) and existence of any hits (the hit pattern) of all the 16 counters and 20 anti-counters are recorded together with the time of the event by the WPU board.

When large inorganic scintillators are used in the space as in the present case, highly ionizing nuclear particles often deposit energy higher than the saturation point of the amplifying system. They may potentially cause some erroneous response in the analog system. In the AE, we install discriminators to detect such events (the upper discriminators) and protect the analog system from such misoperation.

The signal from the 20 anti-counters are processed in units of five in the TPU boards. The outputs of all 20 lower discriminators are distributed to the WPU boards via the "hit pattern" bus. Signals are then summed to produce two sets of pulse height distributions: one has only 4 energy bins but renewed every 1/64 msec, and the other has 64 energy bins and renewed at 512 msec interval. These transient pulse height distributions are used to detect γ-ray bursts, various flare-ups, and other bright transient phenomena. Once a γ-ray burst occurs, for example, the on-board burst detection circuit or the program running in the CPU triggers the memory control circuit of the histogram buffer to record the time-resolved pulse height distributions of the burst for 128 seconds. We expect to detect about 160 bursts per year.

4.2 Pulse Shape Discriminator

The PSD distinguishes events from the two scintillators, the fast-decaying scintillator (GSO) and the slow-decaying scintillator (BGO). There are several PSD methods developed and used in γ-ray astronomy and nuclear physics, one of which being the double shaping method adopted in the HXD. In this method, the signal from a phototube is integrated with two different shaping times and the two output pulse heights are compared. This method is less affected by external electronic noise, while its demerit is that the circuit becomes somewhat complicated. This demerit can be solved by implementing the circuit on an LSI chip.[33] [34] [35] In our LSI chip, the two integration times are set at around τ_{fast} = 100 ns and τ_{slow} = 500 ns.

The outputs of the two shapers have different pulse heights for BGO signals, while they are almost equal for pure GSO signals. The pulse-shape discimination LSI has been developed using a semi-customed LSI technology.[33] [34] [35] Shown in Figs. 12 and 13 is the result of a test done by using the LSI circuit with the phoswich unit of the Engineering Model: the irradiated gamma-rays are from ^{137}Cs (662 keV). In Fig. 12, the linear cluster extending at an angle around 30 deg. to the ordinate, is due to hits on the BGO shielding part while the one extending to right is due to clean hits on the GSO detection part. Compton scattered gamma-rays form two linear clusters bridging between the blob corresponding to the clean hits on GSO and either one of the two blobs corresponding to the bottom BGO and the collimator BGO. One can see that pure GSO events can be seperated from BGO events and Compton scatterd events. Fig. 13 shows how the background is reduced by selection of the GSO cluster in Fig. 12 by the PSD chip and subsequent off-line analysis. Since we have put only one unit in a temperature- controlled box, Compton-scattered gamma-rays escaped or entered through the 3 mm BGO wall as apparent in Fig. 13. In the real detector, these γ-rays will be captured by neighboring units and rejected when the hit pattern is interrogated.

4.3 Digital Electronics

The DE controls acquisition of the data, coordinates among them, detects and reacts on requests for services, and provides the primary interface with the satellite data processor for command and telemetry (see Fig. 11). These tasks are executed by a system consisting of one Intel 80386 running at 8 MHz. To obtain a high data-acquisition rate, each AE board is capable of sending data by the DMA transfer mode to the DE. Here the data for 64 events are blocked so that the interrupt rate to CPU remains low.[9]

The CPU also performs some software event selections by examining the hit pattern around the unit in which the trigger is initiated: this further reduces Compton scattered events and particle interaction events. The CPU acquire calibration data and data used to estimate background.

5 CALIBRATION AND MONITORING

On board calibration will be needed in the energy measurement by the PIN diodes and phoswich detectors. For the diodes, we are examining possiblity of using K X-rays from the phosphorus blonze of the fine collimator. For GSO, the α-rays emitted by a natural isotope ^{152}Gd, appearing at around $E_\gamma \sim 385$ keV with a counting rate around $\sim 10^{-4}$/s/cm^2/keV, will be used.[10] [11] [12] [13] [14]

Critical items to be monitored include various counting rates that will be needed in estimating the activation background. The temperature of the scintillators and phototubes are also to be monitored because of their temperature dependence shown in Fig. 5.

6 EXPECTED BACKGROUNDS

Possible in-orbit backgrounds have been estimated for the present counter design: GSO of $2.4 \times 2.4 \times 0.5$ cm^3 shielded by BGO of ~ 5 cm thickness all around.[22] [8] The proton flux has been assumed to be that of the model given in the reference[23] at the solar minimum, although the scheduled flight time corresponds roughly to the solar maximum when the background is expected to be about half.[23] The results are summarized in Table 2: one can see that the internal and cosmic-ray induced radioactivities will be the dominant source of background below 300 keV. We therefore anticipate that the sensitivity of HXD will be limited by these induced radioactivities.

Among the listed background origins, prompt backgrounds produced by charged particles on BGO can easily be rejected. Gamma-rays generated in passive material around the detector array have some chance to leak through a few centimeter of BGO, if their energy is above ~ 300 keV. We have to minimize passive material close to the HXD detectors, eg. the HXD housing and the fine collimator. Gamma-rays generated

Table 2: Expected background rates

In-orbit activation	:	$\sim (0.5 \sim 1) \times 10^{-5}$ /sec/cm^2/keV at 100 keV
Leak-thru γ-rays	:	$\sim 1 \times 10^{-6}$ /sec/cm^2/keV at 300 keV
		$\sim 2 \times 10^{-5}$ /sec/cm^2/keV at 400 keV
		$\sim 2 \times 10^{-4}$ /sec/cm^2/keV at 500 keV
Off-aperture CXB	:	$\sim 7 \times 10^{-6}$ /sec/cm^2/keV at 50 keV
		$\sim 1 \times 10^{-6}$ /sec/cm^2/keV at 100 keV
Radioactive impurities	:	$5 \sim 1 \times 10^{-6}$ /sec/cm^2/keV below 300 keV

by nuclear interactions in the tip of the XRT complex have some chance to enter the FOV determined by the BGO well.

What may become a dominant background and yet is difficult to estimate is faking of clean-hit GSO events by pile-up of BGO hits or by Cherenkov photons in the PMT face windows. Background due to radioactivity and amount of radioactivity that may be produced have been and still are actively studied by bombarding the materials around the HXD detector with protons and by running the simulation programs.[22] Through these efforts and adequate on board monitoring, we expect to be able to predict the background for actual observations to an accuracy better than $\sim 5\%$. We note that such predictions worked to about $\sim 1\%$ level in the Ginga-LAC.[16]

7 CONCLUSIONS

The design and expected performance of the Hard X-ray Detector (HXD), one of the 3 experiments aboard Astro-E have been presented. Most of its critical elements have been prototyped, tested, and verified their validity. One item that still requires continuing R/D works is the 2 mm thick silicon PIN diodes. The total weight and the total power consumption are to be reduced further. We expect the above issues to be solved within this calendar year.

8 ACKNOWLEDGEMENTS

We wish to thank Dr. H. Ishibashi of Hitachi Chemical Co. Ltd. for collaboration in improving the quality of GSO, Mr. T. Itoh of Bikowski Japan Co. Ltd. for assembly of the BGO wells, Messers K. Taguchi, M. Horii, M. Hamaya, S. Shinoda, and R. Shoumura of Meisei Electronics for detector and electronics assembly, Messers T. Hanazawa, K. Shimizu, and Y. Sano of Fujitsu VLSI Ltd. for the analog LSI design and production, Messers S. Kubo, Kiminori Sato, Keiji Sato, I. Odagi, and Y. Tanaka of Fujitsu Ltd. for the DE part of electronics, and Dr. T. Sumiyoshi of KEK for measuring the reflectivity of the reflector sheets. We acknowledge contributions by Ms. N. Yamasaki, Messers N. Tsuchida, T. Ohtsuka, and K. Nagata to the earlier phase of the R/D works on Astro-E HXD.

The present work was supported by Grant-in-Aid for Scientific Research No. 05242101 and Grant-in-Aid for COE Research No. 07CE2002 by the Ministry of Education, Culture, and Science, Japan.

9 REFERENCES

[1] Inoue, H., *Proc. of the 11th Colloquium on UV and X-Ray Spectroscopy of Astrophysical and Laboratory Plasmas*, Universal Academy Press (Tokyo, 1995)

[2] McCammon, D., et al., *Nucl. Instr. Meth.*, **A326**, 156, (1993)

[3] At present we can only refer to the literature about the ASCA CCDs:
Burke, B. E., et al.,*IEEE Trans. Elect. Dev.*, **38**, 1069, (1991)
Burke, B. E., et al., *IEEE Trans. Nucl. Sci.*, **41**, 375, (1994)

[4] Astro-E XRT if no ref. use ASCA XRT:
Serlemitsos, P., et al., *Publ. Astron. Soc. Japan*, **47**, 105, (1995)

[5] Takagi, K. and Fukazawa, T., *Appl. Phys. Lett.*, **42**, 43 (1983)

[6] Ishibashi, H., Shimizu, K., Susa, K., and Kubota, S., *IEEE Trans. Nucl. Sci.*, **36**, 170 (1989)

[7] Tsuchida, N., Ikeda, M., Kamae, T., and Kokubun, M., *Nucl. Instr. Meth.* submitted (1996)

[8] Kaneda, H., et al., *Proc. SPIE*, **2518**, 85 (1995)

[9] Takahashi, T., et al., *Astrophys. & Astronom.* to be published

[10] Kamae, T., et al.,*Proc. SPIE*, **1734**, 2 (1992)

[11] Takahashi, T., et al.,*Proc. SPIE*, **1734**, 44 (1992)

[12] Kamae, T., et al.,*IEEE Trans. Nucl. Sci.*, **40**, 204 (1993)

[13] Takahashi, T., et al., *IEEE Trans. Nucl. Sci.*, **40**, 890 (1993)

[14] Gunji, S. et al., *Astrophys. Jour.*, **397**, L83 (1992)

[15] Gunji, S. et al., *Astrophys. Jour.*, **428**, 284 (1994)

[16] Hayashida, K., et al., *Publ. Astron. Soc. Japan*, **41**, 373 (1989)

[17] Nakao, K., Senior Thesis, Dept. of Physics, Univ. of Tokyo (1990)

[18] Lewis, T. A., *Nucl. Instr. Meth.*, **A264**, 534 (1987)

[19] For example, BGO crystals supplied by Crismatec.

[20] Baryshevsky, V. G. et al., *Nucl. Instr. Meth.* **B58**, 291 (1991)

[21] Korzhik, M. V., Miesvich, O. V., and Fyodorov, A. A., *Nucl. Instr. Meth.*, **B72**, 499 (1992)

[22] Matsuzaki, K., Master Thesis, Dept. of Physics, Univ. of Tokyo (1995)

[23] Stassinopoulos, E. G., in Rester, Jr., A. C. and Trombka, J. I. (eds.) "High-Energy Radiation Background in Space", AIP Conference Proceedings 186 (1989) p.3

[24] Idesawa, E., Master Thesis, Dept. of Physics, Univ. of Tokyo (1996)

[25] Kobayashi, M. et al., KEK Internal Report **91-1** (1991)

[26] EPO-TEK 301-2 by Epoxy Technology Inc.

[27] KE103 by Shin'Etsu Chemical Inc.

[28] GoreTex Japan Inc., Hyper Sheet Gasket

[29] Kaneda, H., Master Thesis, Dept. of Physics, Univ. of Tokyo (1994)

[30] Tamura, T., Master Thesis, Dept. of Physics, Univ. of Tokyo (1995)

[31] Iyomoto, N., Master Thesis, Dept. of Physics, Univ. of Tokyo (1996)

[32] Sugizaki, Master Thesis, Dept. of Physics, Univ. of Tokyo (1996)

[33] Ezawa, H., et al. *IEEE Trans. Nucl. Sci.* in press

[34] Tsukada, K., et al. *IEEE Trans. Nucl. Sci.* **40**, 724, (1993)

[35] Ezawa, H., Master Thesis, Dept. of Physics, Univ. of Tokyo (1995)